Biophysical Journal Volume 91 September 2006 1619–1629

Ligand Detection and Discrimination by Spatial Relocalization: A Kinase-Phosphatase Segregation Model of TCR Activation

Nigel J. Burroughs,* Zorana Lazic,* and P. Anton van der Merwe†

*Mathematics Institute, University of Warwick, Coventry, United Kingdom; and †Sir William Dunn School of Pathology, Oxford University, Oxford, United Kingdom

ABSTRACT We develop a model of tyrosine phosphorylation and activation of the T-cell receptor (TCR) by localization to regions of close membrane-membrane proximity (close contact) that physically exclude tyrosine phosphatases such as CD45. Phosphatase exclusion generates regions of low phosphatase and high kinase activity and thus our model provides a framework to examine the kinetic segregation model of TCR activation. We incorporate a sequence of activation steps modeling the construction of the signalosome with a final sequestered, or high-stability, signaling state. The residence time of unbound TCRs in tyrosine kinase-rich domains is shown to be too short for accumulation of activation steps, whereas binding to an agonist lengthens the localization time and leads to generation of fully active TCRs. Agonist detection depends only on this localization, and therefore kinetic segregation represents a viable ligand detection mechanism, or signal transduction mechanism across membranes, distinct from receptor oligomerization and conformational change. We examine the degree of discrimination of agonists from a background of null (self) peptides, and from weak agonists achievable by this mechanism.

INTRODUCTION

The mechanism of T-cell receptor (TCR) activation upon agonist binding remains one of the mysteries of T-cell immunology. A number of mechanisms have been proposed, including oligomerization, conformational change, and segregation. Oligomerization models (e.g., dimerization) are based on analogy to tyrosine-kinase-coupled receptors such as the epidermal growth factor receptor. They propose that TCR binding to a specific peptide-major histocompatibility complex (MHC) induces proximity between TCR-associated tyrosine kinases (e.g., Lck) and their substrates. One drawback of oligomerization models is the very low surface density of specific peptide-MHC (pMHC) on cells. The recently proposed pseudodimerization model addresses this by proposing a role for TCR engagement of self-peptide-MHC in oligomerization (1). Conformational change models propose that the TCR undergoes a conformational change in response to agonist binding. Structural studies have largely ruled out conformational changes in TCR$\alpha\beta$ itself as a mechanism but it remains possible that binding leads to conformational changes between TCR$\alpha\beta$ and the associated CD3 complex or between two TCR$\alpha\beta$s in a preformed TCR$\alpha\beta$ dimer. Recent studies have shown that TCR binding leads to a conformational change in the cytoplasmic tail of the CD3ϵ, which enables a proline-rich motif therein to bind Nck (2,3). This change appears to be independent of tyrosine phosphorylation but it remains to be shown whether it is required for TCR activation. Segregation models propose that TCR activation involves redistribution of the TCR and other cell-membrane associated molecules. Specifically, in the kinetic segregation hypothesis (4), regions of close contact form between T-cells and other cells from which molecules with large ectodomains, including the tyrosine phosphatases CD45 and CD148, are excluded. This leads to the creation of a tyrosine kinase-rich domain (KRD) within which tyrosine phosphorylation is favored. TCRs that bind ligand within these regions will be trapped here for long periods, leading to tyrosine phosphorylation of the cytoplasmic portions of the CD3 subunits. Key to the mechanism is the dependence of the TCR/CD3 phosphorylation state on the KRD residence time.

We developed a model to determine the signaling characteristics of the kinetic segregation hypothesis. We use a patterned environment of KRDs within a predominantly phosphatase-rich environment (PRE); thus kinases such as Lck are inactivated (and primed) in the latter, whereas they autoactivate in phosphatase-excluded regions. These KRDs, or phosphatase exclusion regions, are identified with regions of close membrane-membrane proximity (separation 14–15 nm), since the predominant phosphatases have large ectodomains (25–40 nm) and therefore exclusion is energetically favored. Thus, KRDs also function to localize bound TCRs (Fig. 1). Signaling through the TCR involves the stepwise formation of a large multi-molecular complex that has been termed the signalosome (5). One of the earliest events in agonist detection is the phosphorylation of immunotyrosine-based activation motifs (ITAMs) on TCR-associated CD3 chains by Lck, which then recruit and activate the tyrosine kinase ZAP70. ZAP70 phosphorylates the transmembrane adaptor protein LAT, which acts as a scaffold to recruit adaptor proteins and effector proteins including SLP-76, Grb-2, GADs, Sos, and PLCγ1, which are, in turn, further activated by tyrosine kinases including Itk and Tec. Thus, to attain a fully active complex requires a number of phosphorylation and

Submitted January 4, 2006, and accepted for publication May 1, 2006.

Address reprint requests to Nigel J. Burroughs, Mathematics Institute, University of Warwick, Coventry CV4 7AL, UK. E-mail: njb@maths.warwick.ac.uk.

0006-3495/06/09/1619/11 $2.00

doi: 10.1529/biophysj.105.080044

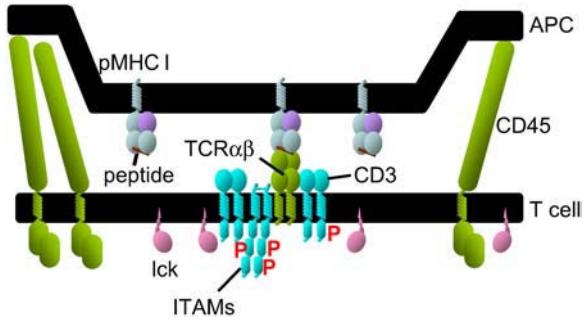

FIGURE 1 A schematic of a region of close contact illustrating CD45 exclusion and kinase activation. Regions of close contact are 15 nm membrane to membrane, whereas CD45 has an extracellular domain of 25–50 nm depending on isoform.

recruitment steps (Fig. 2), a process that has a number of similarities to kinetic proofreading models of signaling and DNA motif discrimination (6–8). Such a sequence of events could therefore underpin ligand specificity within the context of differential localization of bound TCR to regions of close contact. We demonstrate that the residence time of unbound TCRs in the KRDs is very short (milliseconds), and that TCR binding to peptide-MHC significantly lengthens this residence time. For appropriate parameters, a significant number of activation steps can accumulate and thus provide the basis for ligand discrimination and detection. We note, however, that bound TCRs are not absolutely localized to KRDs since they are only localized by a finite energy barrier, and thus leave the KRDs presumably as a state where the membranes are locally distorted, the membranes being more flexible than the actual proteins. However, these excursions out of KRDs are short and do not significantly reduce levels of triggering. We demonstrate that background levels of activation from unbound TCRs and discrimination of weak versus strong agonists relies on both efficient relocation and the activation sequence, the latter functioning as a kinetic proofreading scheme. Further, we incorporate a sequestered, fully activated state that reproduces the observed increase in phosphorylated TCRs on ligand exposure. We interpret this state as a stabilized signalosome.

Mathematically, the initial phases of T-cell activation have not been considered previously. Mathematical models describing the formation of the immunological synapse reproduce the observed large-scale redistribution of TCRs and other molecules (e.g., LFA-1) (9,10) This large-scale segregation is slower than the small-scale segregation that we describe here, and it occurs after TCR triggering. Indeed, synapse models assume upregulation of LFA-1, which follows, and depends on, TCR triggering (11). However, there are some aspects of similarity with these models given their common dependence on differential extracellular domain sizes. The kinase-phosphatase balance as a component in driving TCR triggering has previously been modeled in a feedback context (12,13).

THEORY

Kinase-rich domains

Surface proteins have a range of extracellular domain sizes, from large (>25 nm) for phosphatases CD45 and CD148, through intermediate (10–25 nm) for integrins and coreceptors such as CD4/8, to small (<10 nm) for receptors/ligands such as the TCR, MHC, CD2, CD58, CD128, and B4. Thus on cell-cell contact the membrane separation will be heterogeneous, with most areas separated by >20 nm to accommodate the larger molecules. Small (sub-light microscopy) areas of close contact (14–15 nm) are expected to form under thermal fluctuations or cytoskeleton dynamics, the free energy of the perturbation being reduced by clustering of appropriately sized molecules and bond formation (Fig. 1). These areas of close contact are likely to be unstable (metastable) even though bond formation (CD2-CD58, TCR-pMHC) is favored. It has been suggested that only after TCR triggering

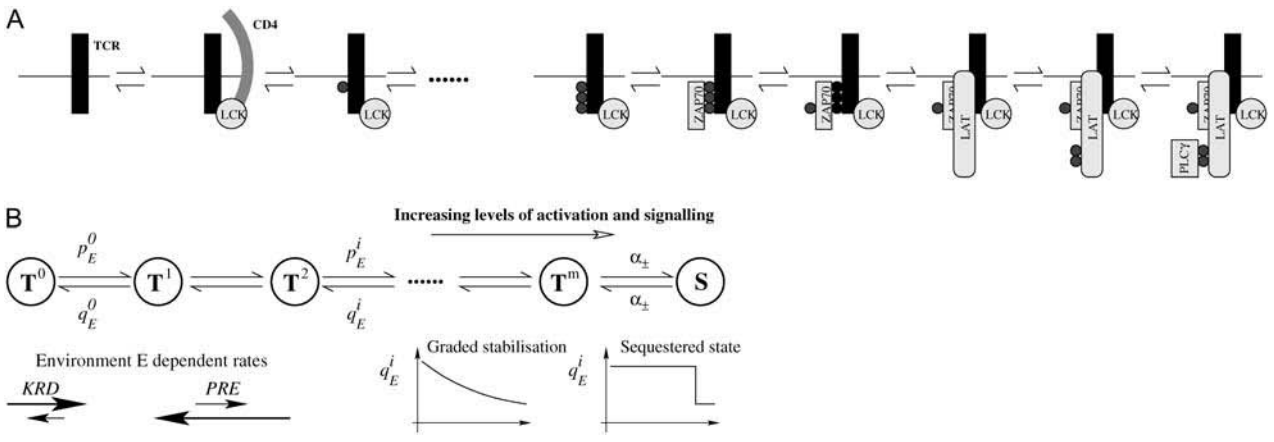

FIGURE 2 (*A*) Schematic for the activation step sequence of events leading to a signaling competent signalosome (● represents tyrosine phosphorylation). (*B*) Mathematical model of activation sequence with trends shown for the event rates in the different environments, (*left inset*), and two models for stabilization of the signalosome through reduced dephosphorylation at high levels of activation (*right inset*). Index *i* labels the activation step and *E* denotes the environment (either KRD or PRE).

is segregation according to size thermodynamically favorable (9), since synapse patternation fails to form in the absence of agonist. These close-contact domains are therefore transient and formed by fluctuation of the intermembrane separation, fluctuations forming a distribution of domain sizes, probably ranging from nanometers to hundreds of nanometers. These regions will exclude the large phosphatases (CD45, CD148) and thus coincide with regions of a high kinase to phosphatase balance of activity, regions, which we call kinase rich domains. We simulate a region of the cell-cell contact interface formed between a T-cell and an antigen-presenting cell. Within this contact interface, we assume there are regions of close membrane proximity (membrane separation ~15 nm) of area fraction f (Fig. 3). We use a static pattern of KRDs, which is justified provided their lifetime is larger than the timescales of the triggering process and the TCR localization time. They will also diffuse in the surface; however, this will have negligible impact on the triggering kinetics and thus can be safely ignored.

Diffusion and localization

Agonist pMHC and TCR are represented as individual molecules that perform a random walk (diffuse) on a lattice patterned with isolated KRDs (Fig. 3), modeled for simplicity as circular discs of radius r. In the absence of binding, both MHC and TCR diffuse randomly, but when bound, the complex diffuses in a potential determined by the local membrane-membrane separation, i.e., there is a potential difference Φ between a KRD and the phosphatase-rich environment for a bound TCR-pMHC complex. To estimate Φ, we model bonds as springs (9,14), with natural bond length l and elasticity κ to give $\Phi(x) = \frac{1}{2}\kappa(z(x) - l)^2$, where $z(x)$ is the membrane-to-membrane distance in the contact interface at position x. Thus, the ratio of bond affinities between KRDs and the PRE is $\exp(\Phi/kT)$, where $\Phi = \frac{1}{2}\kappa\Delta l^2$ and Δl is the difference in membrane separations between the two regions. Since the TCR-pMHC bond does not break under application of a pN force, we assume for simplicity that the off-rate is identical in the two environments, i.e.,

$$k_{\mathrm{on(PRE)}} = k_{\mathrm{on(KRD)}}\exp(-\Phi/kT),\ k_{\mathrm{off(KRD)}} = k_{\mathrm{off(PRE)}}. \qquad (1)$$

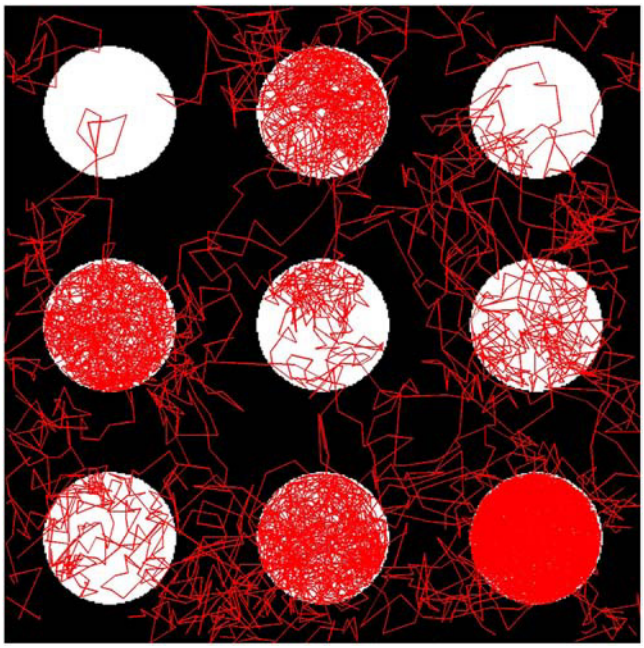

FIGURE 3 Typical trajectory for an agonist-MHC. The KRD pattern consists of nine KRDs (*white*) of radius $r = 103$ nm on a regular grid. Size simulated is 1 μm^2 with cyclic boundary conditions. Particle position shown every 5 ms for 50 s.

The results are in fact not strongly sensitive to this assumption. A bound TCR will experience a free energy barrier at the KRD/PRE boundary; thus, in the random walk simulation of a bound complex, a move from a KRD to the PRE is accepted with probability $\exp(-\Phi/kT)$. Both migration and reaction kinetics thus generate a relative complex density of $e^{-\Phi/kT}$.

The same principles can be used to compute the depletion of CD45 in the KRDs, i.e., phosphatase activity is reduced by $e^{-\Phi'/kT}$ in KRDs, where $\Phi' \approx \Phi$ is the difference between the chemical potentials of a CD45 molecule in the two environments. However, it has been proposed that CD45 has an active and an inactive state, whereas Lck activation is nonlinear (autoactivation) and requires priming by CD45, effects not determined by these assumptions. Because of this, we assume that kinase and phosphatase activities are independent in the two environments. We do not explicitly model CD45 molecules or Lck, but assume that these are at sufficiently high concentration that concentration fluctuations are negligible.

Activation dynamics

We model TCR triggering as a sequence of states, effectively a reversible kinetic proofreading scheme of length m (Fig. 2 *B*), where a step is either a tyrosine phosphorylation or recruitment of a component of the signalosome (5). For instance, earlier steps may correspond to ITAM phosphorylation or kinase recruitment (ZAP70, Lck), and later steps to recruitment and phosphorylation of adaptors (e.g., LAT, SLP-76, Grb2) and effector proteins (e.g., phospholipaseCγ1). The rates of these activation steps depend on the environment; thus, in a KRD the activation rate $\tilde{p}$ is high, whereas there is a low rate of reversion $\tilde{q}$, and in the PRE scheme the corresponding rates are p and q with $q \gg p$ (Fig. 2, Table 1). This environment dependence strictly relates to phosphorylation steps, since the two environments only differ in efficiency of kinases and phosphatases; hence, we are assuming that there are a number of key rate-limiting phosphorylation steps in the construction of the signalosome. For specificity to arise from this sequence of steps they must also have similar rates, a likely consequence of the fact that the same kinase is probably responsible for subsequent steps. Thus, our model is simplified in that the rates of subsequent steps are all assumed equal (faster steps are ignored) and events are assumed independent. We also modify the activation sequence by incorporating a final ''sequestered'' state (Fig. 2), corresponding, for example, to the formation of an enlarged fully competent signaling complex of adaptors and kinases where cooperative binding within the signalosome decreases the rate of signalosome decay/unbinding. Other models with a gradual increase of stability of later stages in the activation sequence, or unequal rates of (in)activation are likely to give similar results. Note that the pMHC unbinding rate is not influenced by the activation state of the TCR; thus, coreceptor recruitment is not explicitly included as part of the activation sequence. We justify this either by modeling activation in the absence of coreceptors, or, when coreceptors are present, they are in excess and thus MHC is predominantly already bound to CD4/CD8.

A plausible length m for the activation sequence is 10 based upon the known sequence of steps. Theory suggests, however, that the dependence on length is weak once above 3, provided the rates are suitably rescaled (15). For reversible kinetic proofreading schemes with $m > 3$ the probability of reaching the end of the sequence instead of unbinding, and thus achieving full activation, is approximately $\exp -\beta k_{\mathrm{off}}$, where $\beta = m/(\tilde{p} - \tilde{q})$ for a TCR that remains in the KRD environment (high Φ). Thus, under variation of the length m of the sequence the rates of the intervening steps should be rescaled by m to preserve the sensitivity, i.e., $p, q, \tilde{p}, \tilde{q} \propto m$ etc. Accordingly, the mean time to reach the end of the sequence conditioned on not unbinding is conserved, whereas the variance of this time decreases as m^{-1}. For an agonist with a lifetime of 10 s, $k_{\mathrm{off}} = 0.1\ \mathrm{s}^{-1}$, we fix this probability at $e^{-1} \approx 0.367$, thereby determining the scale of β. This implies that in TCR excess, the triggering rate of a pMHC agonist is $k_{\mathrm{off}} \exp -\beta k_{\mathrm{off}}$, and thus maximal at $k_{\mathrm{off}} = \beta^{-1} \approx 0.1\ \mathrm{s}^{-1}$. In the simulations we use $m = 10$, although all sufficiently large m give similar results (not shown). To complete determination of the model, we need to determine appropriate values for p and q. Dephosphorylation rates in the PRE must be sufficiently large to

reduce levels of activation in the absence of agonist; in fact, in signal interruption studies using specific kinase inhibitors or blocking antibodies, tyrosine phosphorylation is lost within a minute, indicating that dephosphorylation is rapid (16,17). We also assume that although KRDs are predominantly kinase active regions, kinase activity is also present in the PRE, whereas phosphatases cannot be absolutely excluded from KRDs. We illustrate our model under relative kinase/phosphatase activities varying only by two orders of magnitude (Table 1).

The high stability of the final sequestered state is achieved with a low inactivation rate $\alpha_- \ll q$, a half-life of 5 min, and a binding rate α_+ on a scale of seconds, both independent of the environment. The lifetime was set to match TCR down-modulation timescales (18). This is reasonable given that only triggered TCRs are likely to be downmodulated, whereas TCRs remain marked for downmodulation after dissociation from pMHC (18,19). If all triggered TCRs are not downregulated, i.e., if there is a probability of inactivation (20), the sequestered state lifetime will be <5 min.

Self-peptides

We do not explicitly model self-pMHC molecules, since they are at high density. We used a uniform fixed density of unbound self-pMHC, M_{self}; thus, unbound TCRs have a constant rate $k_{on}M_{self}$ of binding to self. In the simulations, all self-pMHC have the same off rate (3 s^{-1} or 5 s^{-1}), i.e., we only model the most stable peptide component (longest half-life) for simplicity. We use three self-profiles for illustration: self, with $k_{off} = 3\ s^{-1}$ at density 50 μm^{-2}; low-activity self, with $k_{off} = 5\ s^{-1}$ at density 300 μm^{-2}; and high-density self, with $k_{off} = 3\ s^{-1}$ at density 300 μm^{-2}. The first two are likely to be representative of typical antigen presenting cells, whereas the latter is used here to allow trends to be observed (i.e., triggering levels are high enough to be visible) and thus compared to agonist triggering rates.

RESULTS

We simulate early signaling on initial contact of a T-cell with an antigen-presenting cell, using a fixed area of contact (1 μm^2) for illustration of the activation characteristics. An agonist-pMHC rapidly visits KRDs (millisecond scale), being clearly trapped when bound (Fig. 3). We observe an increase of triggered TCRs on a scale of minutes (Fig. 4). Since the probability of activation per binding is at most ~30%, ($k_{off} = 0.1\ s^{-1}$), the average rate of triggering of a single pMHC is at most two per minute, thereby determining the timescale. As fully activated TCRs are assumed to inactivate (or be downregulated) with a half-life of 5 min (α_-^{-1}), the number of activated TCRs saturates at a level of 10–15 per pMHC on achieving equilibrium, a small fraction of the total TCR pool (30,000 per cell (18)). Without the stabilization of the final state, fully activated TCRs have a very short lifetime when released from the MHC, since they diffuse into the PRE where phosphatase activity is high. In these circumstances, although TCR triggering is high under agonist exposure, the density of fully activated TCRs is negligible; in fact, in the absence of stabilization of the final state we observed a fully activated TCR fraction of only 0.25% at an agonist density of 1 μm^{-2}, compared to up to 15% with a stabilized final state.

The interplay between the spatial segregation of kinase and phosphatase activity and localization to kinase-rich domains of bound TCRs in determining triggering is illustrated in the single-molecule time series of Fig. 5. Free TCRs and pMHC diffuse throughout the interface with rapid transitions between KRDs and PRE (timescales of milliseconds with 100-nm-sized KRDs). However, on binding, the TCR-pMHC complex remains on a scale of seconds in KRDs, and although excursions to the PRE occur, they have a negligible effect on activation, causing only occasional collapse of the activation state (Fig. 5). These excursions will have a greater impact as Φ, D decrease, or q increases.

There are three contributions to the cell activation signal: a contribution from unbound TCRs being activated by traversing the KRDs (background), a contribution from nonspecific binding to self-peptides (self), and the specific signal

TABLE 1 Default parameter values

Parameter	Symbol	Value
KRD area fraction	f	0.3
KRD radius	r	103 nm
TCR density (total)*	T	100 μm^{-2}
Self MHC density (free)	M_{self}	300 μm^{-2}
Diffusion coefficient (36)	D	0.1 $\mu m^2 s^{-1}$
TCR-pMHC binding rate in KRDs	k_{on}	0.005 $\mu m^2 s^{-1}$
Unbinding rate (good agonist) (22)	k_{off}	0.1 s^{-1}
Unbinding rate (self)	–	3. s^{-1}
Localization potential	Φ	$5kT$
Activation sequence length	m	10
Phosphorylation rate (PRE)	p	0.5 s^{-1}
Phosphorylation rate (KRD)	$\tilde{p}$	2.25 s^{-1}
Dephosphorylation rate (PRE)	q	60 s^{-1}
Dephosphorylation rate (KRD)†	$\tilde{q}$	0.25 s^{-1}
Sequestered state activation rate	α_+	10 s^{-1}
Sequestered state inactivation rate	α_-	0.003 s^{-1}
Lattice size	–	400 × 400
Simulation area	–	1 μm^2

*This corresponds to 100 TCRs in the simulation.
†The effective concentration exclusion potential is $\Phi' = 5.5kT$.

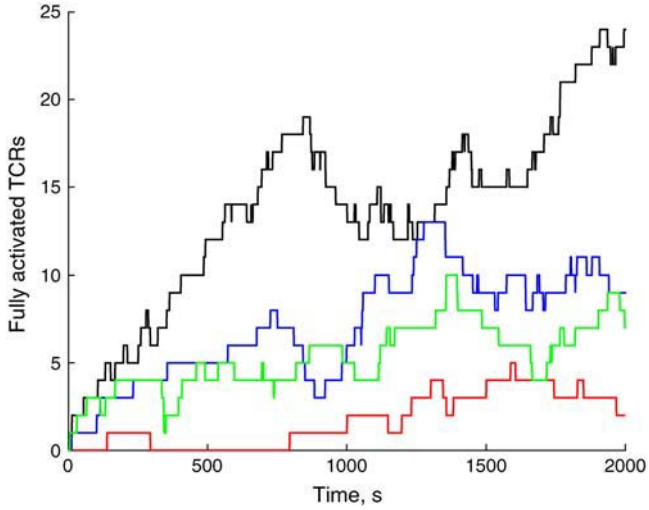

FIGURE 4 Triggering time series (number of fully assembled signalosomes). High-density self (300 μm^{-2}, $k_{off} = 3\ s^{-1}$) in red, agonist, $k_{off} = 0.1\ s^{-1}$ (*black*), $k_{off} = 0.7\ s^{-1}$ (*green*), and $k_{off} = 0.01\ s^{-1}$ (*blue*). Parameters are as in Table 1.

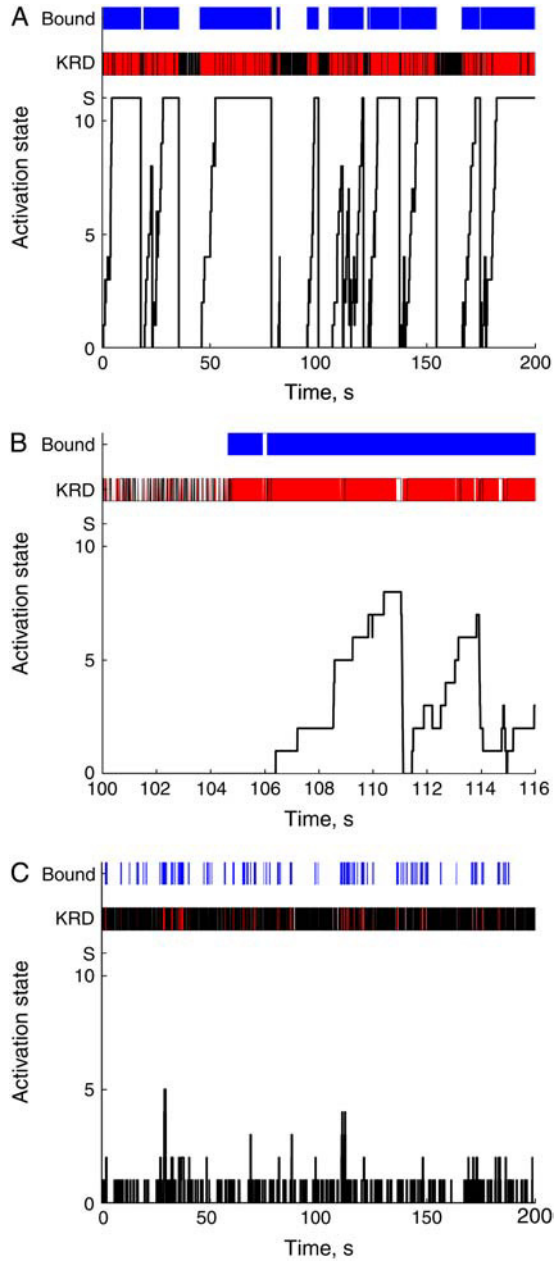

FIGURE 5 Single MHC triggering time series and the correlation of activation with the environment and binding. (*A*) Agonist-MHC. (*B*) Enlargement of *A* over a time period of 100–116 s highlighting loss of activation on excursion to the PRE. (*C*) Tracking of a TCR in the presence of (high-density) self. Periods of binding with TCR are shown in blue, and periods while in KRDs are shown in red. Rapid excursions between regions appear black (see time enlargement *B* showing fine detail of excursions in *A*). The activation state of the bound TCR (*A* and *B*) and TCR (*C*) are shown. *S* denotes the sequestered state. Parameters are as in Table 1.

from agonist pMHC. This gives a combined triggering rate $\lambda = \lambda_{\text{backgnd}} + \lambda_{\text{self}} + \lambda_{\text{agonist}}$. For efficient agonist detection, the signal from a good agonist λ_{agonist} must be clearly distinguishable from background signaling λ_{backgnd} and from self λ_{self}. To illustrate the determinants of self-triggering we will use an unrealistically active self-peptide profile, specifically high-density self, with $k_{\text{off}} = 3\ \text{s}^{-1}$ at a density of 300 μm^{-2}. This would mean that 100,000 MHC, or 10–50% using 200,000 to 1,000,000 MHC per cell, are loaded with peptides with $k_{\text{off}} = 3\ \text{s}^{-1}$. More realistic profiles are self, with $k_{\text{off}} = 3\ \text{s}^{-1}$ at a density of 50 μm^{-2}, and low-activity self, with $k_{\text{off}} = 5\ \text{s}^{-1}$ at a density of 300 μm^{-2}. For the parameters chosen in Table 1, the model clearly demonstrates that a single agonist pMHC has a triggering rate above background levels and populations of self (neutral) peptides (Figs. 4 and 6). The shift of occupancy to higher activity states in the presence of peptides (self or agonist) is shown in Fig. 6. The two realistic self profiles, self and low-activity self, show a similar distribution among the partially active states, demonstrating that both peptide quality and density play a role in self, whereas the fully

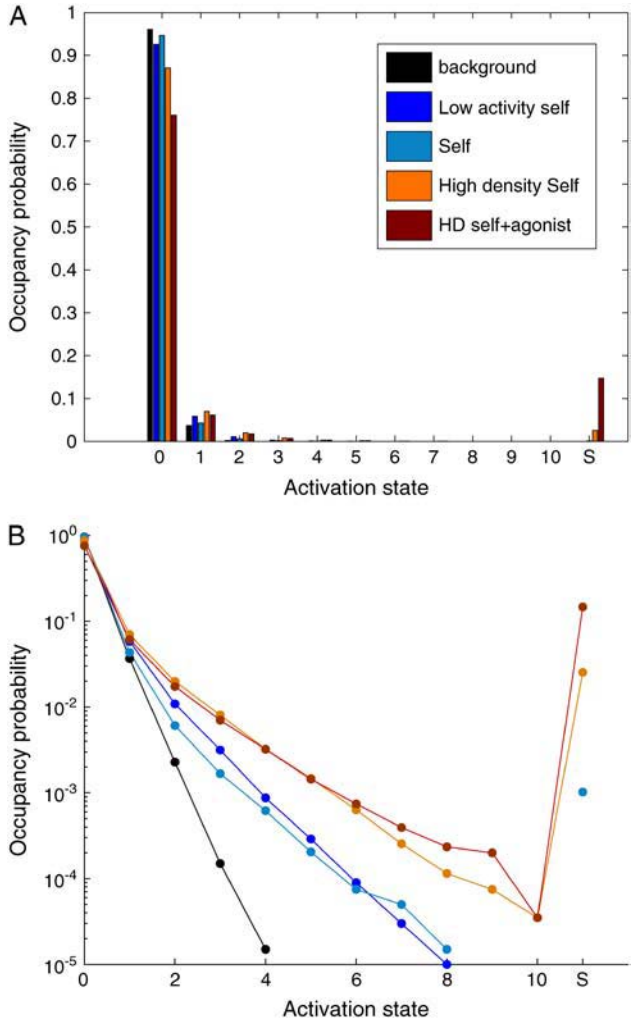

FIGURE 6 Activation-state occupancy for background (no MHC), low-activity self ($k_{\text{off}} = 5\ \text{s}^{-1}$ at 300 μm^{-2}), self ($k_{\text{off}} = 3\ \text{s}^{-1}$ at 50 μm^{-2}), high-density self ($k_{\text{off}} = 3\ \text{s}^{-1}$ at 300 μm^{-2}), and agonist ($k_{\text{off}} = 0.1\ \text{s}^{-1}$ at 1 μm^{-2}) with high-density self. (*B*) Same as *A* in log scale, same colors. Results are based on the first 2000 s of a single run per case and probabilities $<10^{-5}$ are not shown.

active state is only occupied with more stable self-peptides (high-density self) (Fig. 6). These self and background triggering rates have to be scaled by the appropriate contact area to obtain the triggering for a contact. Typical areas of contact are on a scale of 10 μm^2; thus, a single peptide agonist would still give significant triggering relative to realistic self-peptide profiles (multiplying self or low-activity self by 10 relative to Fig. 6), although self is still likely to generate fully triggered TCRs with our parameters. Background triggering on the free surface of the T-cell will be negligible, since KRDs are absent.

The activation occupancy profile is geometric, i.e., the relative occupancies from state k to $k + 1$ are in a constant ratio γ (except for the final sequestered state) (Fig. 6). This is similar to that observed in kinetic proofreading schemes and follows from the assumed independence of the kinase and phosphatase kinetic rates with position k in the activation sequence of Fig. 2. In the case of background triggering, the fraction of time spent in KRDs is in fact f, the KRD area fraction, because there is no preference for either environment. The ratio γ is then the ratio of phosphorylation to dephosphorylation rates averaged over the environment, $(1-f)p+f\tilde{p}$ and $(1-f)q+f\tilde{q}$, respectively. Thus, despite a large population of $N \sim 30000$ TCRs per cell, the background signal is easily controlled; both an increase in the length of the kinetic proofreading scheme m, or a decrease of γ, by either increasing the dephosphorylation rate in the PRE or reducing the fraction of KRDs, are effective in reducing the background signal. Note that γ should be small for a low level of activation in the absence of agonists, and thus the constraint $\tilde{p} < q$ follows, as f cannot be negligible, i.e., the dephosphorylation rate in the PRE is faster than tyrosine phosphorylation in KRDs. The most effective reduction, without compromising agonist detection, is through increasing the dephosphorylation rate q, e.g., high CD45 activity, and increasing the length m. With the parameters of Table 1, the background triggering rate is $<10^{-14}\ \mu m^{-2}\ s^{-1}$ with $\gamma = 0.024$.

A second key attribute of T-cell activation is the ability to discriminate peptides, essentially discriminating between agonists with different off-rates k_{off} (21,22). Although feedback (13,23) and signal integration (16) may play a role in differentiating agonists, there must be differences in the signal at its source, i.e., in the rates of triggering. We find good levels of discrimination between agonists with off rates 0.01, 0.1, and 1.0 s^{-1}, whereas agonists with $k_{off} \approx 0.1\ s^{-1}$ are optimal (Fig. 7). Longer half-lives decrease activation, eventually plateauing at one triggered TCR per pMHC for half-lives of 1000 s (Fig. 7). This reflects the importance of serial triggering (18) to T-cell activation; in this case, the pMHC fails to exchange TCRs, remaining bound to the same (activated) TCR. Self, being comprised of a high number of poor binding peptides is effectively controlled because the residence time of bound complexes in KRDs remains small because of rapid TCR exchange. In contrast to background signals from

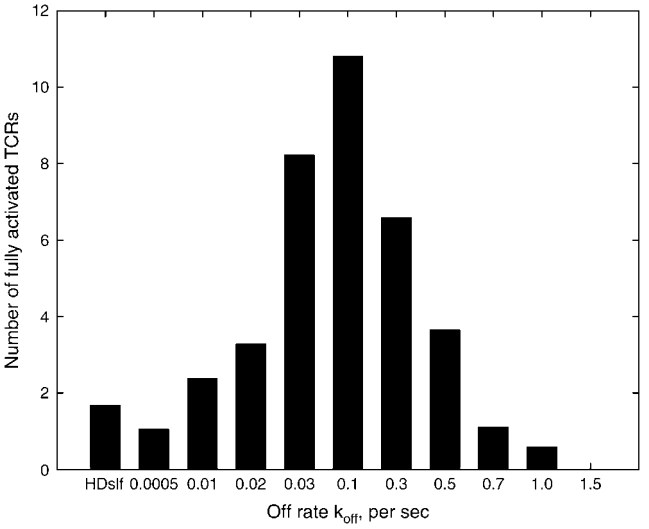

FIGURE 7 Average number of activated TCRs over the first 2000 s under variation of agonist quality (k_{off}). In these simulations, self is absent ($M_{self} = 0$), other parameters are as in Table 1. High-density self (*HDslf*) alone is shown for comparison.

unbound TCRs, triggering by self has the same dependencies on model parameters as agonist signaling; thus, in particular, it cannot be reduced by continually increasing the sequence length m (unless sensitivity is reduced (24)).

An approximation for the triggering rate can be derived for long activation sequences m. Assuming that bound TCRs remain localized in KRDs for the duration of binding (large trapping potential Φ), the triggering rate for an agonist $\lambda_{agonist}$ is given by $k_{off}\ k_{on}[T]fe^{-\beta k_{off}}/(k_{off}+k_{on}[T]f)$, where $[T]$ is the free TCR density and $\beta = m/(\tilde{p}-\tilde{q})$, with a corresponding queue equilibrium $\lambda_{agonist}/\alpha_{-}$. Here we assume the number of agonists is small so that we can ignore TCR competition; the free TCR density is therefore approximately equal to the TCR surface density. We also ignore the time to enter the final sequestered state. These expressions clearly demonstrate that the fraction f must not be negligible for agonist detection; specifically, fractions f as low as $k_{off}/k_{on}[T] \sim 20\%$ will cause a reduction in signaling. For finite Φ, a time-averaged kinase and phosphatase activity can be used to derive an appropriate approximation. These approximations give reasonable fits to the data (not shown), and capture the essential qualitative features.

Environment heterogenity also affects signaling characteristics; both the strength of the trapping potential Φ and the size of the KRDs affect signaling. If the trapping potential is insufficiently high, bound TCRs spend sufficient time in the PRE to become inactivated and the triggering rate falls (Fig. 8 *A*), whereas at high potentials triggering becomes independent of Φ. Similarly, as KRD size increases, triggering increases because bound TCRs remain longer in a KRD (Fig. 8 *B*). However, self and background signals also increase, as shown in Fig. 8 with high-density self, reducing the ability to filter nonspecific (relative) signals. KRD size only affects

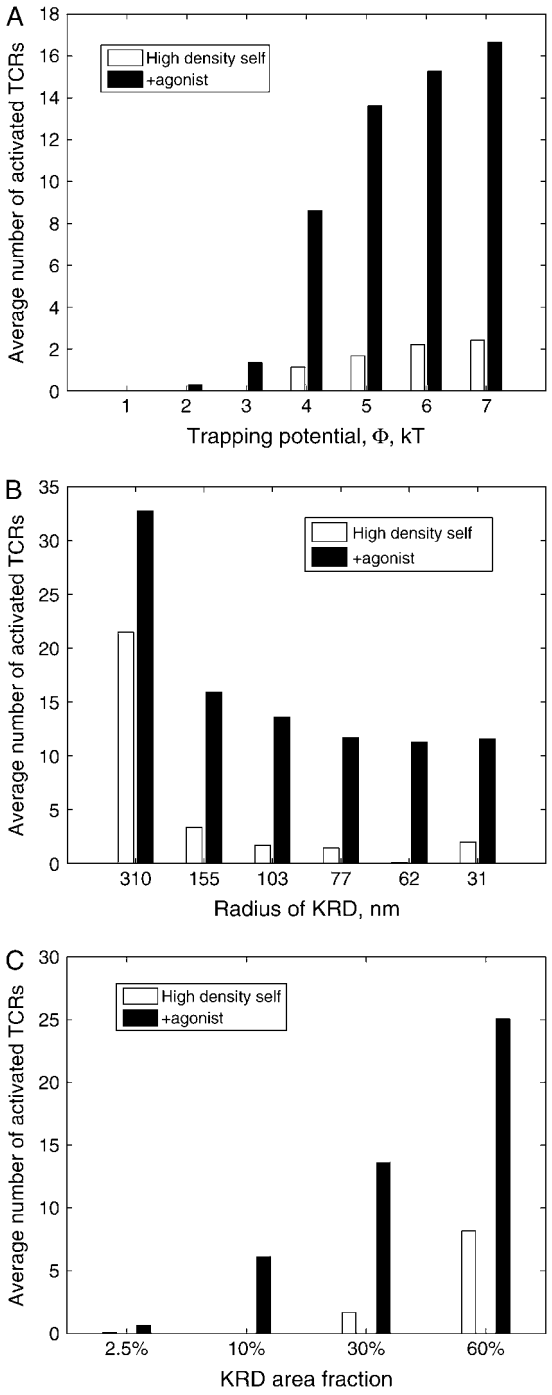

FIGURE 8 Average number of activated TCRs over the first 2000 s under variation of (*A*) trapping potential Φ, (*B*) KRD radius (area fraction of KRDs remains 30%), and (*C*) KRD area fraction *f*. The number of KRDs in *B* are 1, 4, 9, 16, 25, and 100, respectively. The two cases are high-density self (*open bars*) and high-density self plus agonist (*solid bars*). Unvaried parameters as in Table 1.

triggering above a certain threshold that depends on the trapping potential Φ and activation rates. This can be explained from a consideration of the relative timescales. We find that localization of the bound complex, although significant compared to unbound TCRs, is far from absolute, and TCR-pMHC complexes escape from the KRDs on timescales significantly shorter than 10 s (optimal agonist complex lifetime). For instance, KRDs with localization potentials $\Phi = 1, 2, 3, 5, 7$, and $10kT$ have mean residence times of 0.005, 0.015, 0.04, 0.3, 2.1, and 45 s, respectively, whereas for $\Phi = 15kT$, the residence time in excess of 1000 s. In contrast, the majority of excursions from KRDs are very short, mean 4.5 ms, and thus only when the excursion frequency is sufficiently high is signaling reduced. This compares to phosphorylation in KRDs and dephosphorylation in the PRE with timescales of 0.5 s and 0.02 s, respectively. Therefore, for $\Phi < 5$, bound TCRs experience an average kinase-phosphatase environment, and isolated events of localization to a KRD are of insufficient duration to induce a single activation step. However, for $\Phi = 7$ and above, localization to a KRD will on average increase activation levels by more than one activation step. The KRD localization duration relative to the activation timescale provides an explanation for the enhanced triggering rate observed on larger domains (Fig. 8).

The dependence on KRD size and the trapping potential Φ for efficient ligand detection are interdependent. This follows from an analysis of the residence time of unbound TCRs and bound complexes in KRDs (Fig. 9). Since the system is stochastic, there is a distribution of residence times that should be compared to the exponential distribution for the lifetime of the TCR-pMHC complex $Exp(k_{\text{off}})$ to assess probable event sequences. Escape from a localized potential can be explained by a rough argument as follows. At each attempt of the TCR-pMHC complex to cross the KRD boundary, there is a probability of success of $e^{-\Phi}$ (setting $kT = 1$). Diffusion gives a space-time dependence of $x_{\text{rms}}^2 = 4Dt$ (root mean-square distance); thus, the frequency of attempts to cross the boundary has a dependence cD/r^2 (where c is a constant), which can clearly be very high for small domains. In time t,

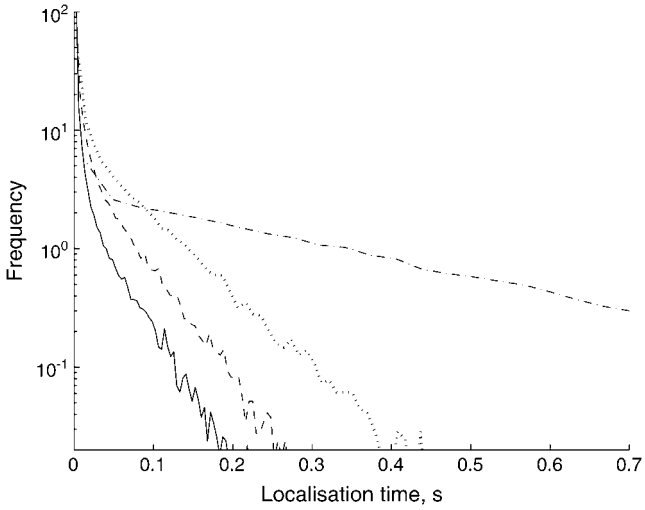

FIGURE 9 Localization time in a KRD of a bound complex, with $\Phi = 1$, 2, 3, and $5kT$ (*solid*, *dashed*, *dotted*, and *dot-dashed lines*, respectively).

there are therefore cDt/r^2 attempts; provided this is large, we obtain the probability of no escape by time t as

$$(1 - e^{-\Phi})^{\frac{cDt}{r^2}} \approx \exp - \left(\frac{cDt}{r^2} e^{-\Phi}\right). \quad (2)$$

This is an exponential distribution (cf. Fig. 9) with mean time to escape $r^2 e^{\Phi}/(cD)$ with $c \approx 50$ from numerics; thus, smaller domains require higher trapping potentials to achieve the same level of localization. Using this relation, we find that for a TCR-agonist pMHC complex to reside in the KRD for its lifetime (10 s) requires a KRD size of order $\sqrt{e^{-\Phi} cD/k_{\text{off}}} = 7e^{-\frac{1}{2}\Phi}\,\mu$m, or ~700 nm for $\Phi = 5kT$, whereas to remain in a KRD for 0.5 s (kinase phosphorylation timescale) requires a KRD size of 150 nm. Thus, KRD size-enhanced triggering will occur for KRDs with radii >75 nm (Fig. 8 *B*).

Finally, we examine the requirements on the area fraction f. Since TCR-pMHC complexes form most efficiently in KRDs, ligand detection decreases as f decreases; however, since the PRE damps activation in the absence of agonists, a large area fraction f also results in poor discrimination since the self contribution is large (Fig. 8 *C*). This can be compensated by increasing the phosphatase efficiency in the PRE, i.e., there is no particular area fraction selected by the dynamics except that it cannot be negligible or agonist triggering will be negligible, and must be <100%.

DISCUSSION

In this article, we have examined the kinetic segregation hypothesis and shown that TCR activation under agonist exposure can be a sole consequence of an extended localization time of bound TCRs to kinase-rich domains. Our model demonstrates that even with a single agonist MHC we obtain a small but significant number of triggered TCRs, of the order of 15 after a transient lasting 10 min (Fig. 4). At higher agonist-pMHC density the effects will be additive until competition for TCR binding sets in, or a key signalosome component becomes limiting, e.g., the kinase Lck (25). This timescale is determined by the triggering rate, two activated TCRs per agonist per minute, and the inactivation rate, 0.2 per minute, whereas the timing of cell responses will depend on where thresholds are set and on what variables (15). Our model thus provides a basis for ligand detection distinct from the traditional mechanisms of conformational change or dimerization, a mechanism that isn't limited to the immunological context discussed here. For efficient agonist detection, we identify three crucial properties:

Efficient segregation of kinases and phosphatases, with faster dephosphorylation in the phosphatase-rich environment than phosphorylation in kinase-rich domains ($\tilde{q} > p$). In fact, only phosphatase exclusion is necessary, i.e., kinase activity can be uniform $p = \tilde{p}$ (not shown).

An underlying activation cascade (similar to the reversible kinetic proofreading scheme used here) to provide the basis of agonist discrimination and background triggering suppression. This activation through a sequence of steps introduces a time delay to signaling competency and thus a sensitive dependence to the TCR-pMHC complex half-life (or rate k_{off}).

Protection of fully activated TCRs (signalosomes) from phosphatases to allow accumulation of functional signaling TCRs, or some other method of signal integration. Accumulation of activated TCRs through dephosphorylation protection reproduces the hall-marks of serial triggering (18).

We demonstrated this mechanism with a 240-fold difference in dephosphorylation rates between the PRE and KRDs, of the same order as the segregation energy potential, $e^{\Phi'} = 240$ with $\Phi' = 5.5kT$, as required for consistency (see discussion in Theory). There are, however, other cytoplasmic phosphatases implicated in TCR triggering that would not be excluded from regions of close contact. Our exclusion criterion refers to phosphatase activity targeting certain key substrates critical for TCR triggering. It is plausible that this specific phosphatase activity is decreased by such an amount for the following reasons. First, CD45 is exceptionally abundant, comprising >10% of the T-cell surface (26) and >90% of the membrane-associated tyrosine phosphatase activity (27). Second, tyrosine phosphatases show exquisite substrate specificity when expressed at normal levels in their normal environment (28), making it unlikely that other phosphatases can efficiently substitute for CD45. Clear evidence for this is that T-cells deficient in CD45 show profound defects, demonstrating that other tyrosine phosphatases are not able to substitute for CD45 (29). Finally, we have not optimized this model; thus, the limits on the parameters for functionality are not at present known and a phosphatase activity difference <240 may well be possible. However, to validate an analysis of this type, the specificity and sensitivity properties for early TCR triggering need to be determined, specificity most likely being function-dependent and thus differing between cytokine secretion and early signals (15). Our analysis also indicated a dependence on KRD size above a certain threshold; for our parameter values, this large domain enhancement occurred for domains >100 nm in radius. However, for particular parameter regimes, triggering could be solely dependent on this enhancement, i.e., small domains could produce negligible triggering. Otherwise, the system is robust to a reasonable level of variability between cells, but extreme variations in area fraction or kinase or phosphatase densities disrupt ligand detection.

A number of T-cell activation dependencies can be explained by our model. First, truncation of the ectodomain of tyrosine phosphatases CD45 and CD148 inhibits TCR triggering (30,31), exclusion and segregation being less effective in this case. Second, activation has a dependence on the

KRD patternation. Significantly, as the kinase-rich domains increase in size—for instance, as they coalesce in the immunological synapse—activation signals would increase and the ability to filter out signals from null peptides decreases. Contributions to the signals from null peptides has been observed in the synapse (32); our model suggests that this contribution only arises from large KRDs. Third, the coreceptors CD4 and CD8, by stabilizing the TCR-pMHC complex and localizing the kinase Lck with the TCR, are likely to increase the residence time of bound TCRs to KRDs and also increase the rate of early signalosome activation steps and thus increase signaling. Fourth, it has recently been shown that progressively increasing the size of the pMHC abrogates TCR triggering (33). It was proposed, with some supporting evidence, that this was the result of an increase in intermembrane distance in the region of TCR engagement of pMHC, which resulted in less effective exclusion of CD45 from this region. The model presented here suggests an additional mechanism, namely, less effective trapping of elongated TCR-pMHC within the KRD. The model predicts that the potential energy barrier preventing diffusion of engaged TCR-pMHC complexes will be strongly dependent on changes in TCR-pMHC dimensions.

The essential requirement for achieving differential signaling between unbound and bound TCRs is the segregation of bound TCRs from phosphatases. Our model uses the ingredients of the kinetic segregation hypothesis (4). However, the key mechanism of CD45 exclusion from regions of close contact through its large extracellular domain size also suggests that CD45 access to bound TCRs may be reduced compared to access to unbound TCRs or, more specifically, that a bound TCR can generate its own kinase-rich shell environment (in analogy to lipid shells (34)). Here, the distinction is between local membrane distortion around the single TCR-pMHC complex compared to a region of close contact on a larger scale ($>$10 nm) and stabilized by other molecules, e.g., coreceptors such as CD2-CD58. This suggests that the event of TCR binding alone is sufficient to exclude CD45 from the local bond proximity, reducing phosphatase access and thus reducing TCR dephosphorylation. Lck may also autoactivate within the shell, leading to TCR tyrosine phosphorylation. This model would display triggering characteristics similar to those described here (not shown), but without the requirement for spatial segregation/patternation if we assume that bound TCRs generate a local kinase-dominant environment similar to that of larger KRDs. In contrast to the kinetic segregation relocation mechanism, there is a direct correlation between binding and phosphorylation in this case. However, there are a number of arguments against this assumption. First, local membrane distortion around a single TCR-pMHC bond produces graded levels of exclusion; thus, CD45 exclusion will be less efficient as the signalosome grows in size, and will never be as effective as a larger KRD where cooperative effects mean that the TCR is highly protected within the body of the KRD. Kinase activity may also be reduced in kinase-rich shells relative to larger KRDs. Second, the cell membranes apply a pulling force to the bond, which in larger KRDs is shared among any bonds in the domain. This is likely to reduce the half-life of the bond and thus reduce the triggering, which is very dependent on complex stability. In our simulations, we assumed that k_{off} was not affected by the intermembrane separation (Eq. 1) or the application of a pulling force on the TCR-pMHC complex. For KRDs, this assumption could be relaxed. A 50:50 split of the effects of the potential Φ between the on- and off-rates in the KRD segegration model, ($k_{\mathrm{on(PRE)}} = k_{\mathrm{on(KRD)}} \exp(-\Phi/2kT)$, $k_{\mathrm{off(KRD)}} = k_{\mathrm{off(PRE)}} \exp(-\Phi/2kT)$), was found to have a negligible effect on the agonist and self signals. This is because excursions of bound TCRs are short in the PRE (milliseconds). We conclude that signaling from TCRs in the absence of KRDs is likely to be inefficient because of these effects. We suspect that formation of a kinase-rich shell by bound TCRs in the PRE may enhance the early steps in the activation cascade, whereas as the developing signalosome increases in size phosphatase access increases, giving a much stronger requirement for finite-size KRDs for later steps in the activation sequence. This suggests that the early phosphorylation of CD3 may not be as dependent on kinase-rich domains as the construction of a fully competent signalosome.

A number of our assumptions do not affect our results. We used a simple reversible activation sequence that possessed kinetic proofreading characteristics. The exact structure of the activation sequence is not important and other models will give similar results provided it retains specificity; in fact, we argue that sequences with $m > 3$ all give similar results. Activation steps can be unequal in importance (the slowest steps determining the specificity properties, i.e., m is the number of rate-limiting steps), for instance, the first couple of tyrosine phosphorylations may be easily acquired, which would raise the average phosphorylation state of the background. In fact, background phosphorylation is observed in the absence of agonist (35); this, however, is not an argument against kinetic proofreading. In addition, dephosphorylation steps can be grouped (multiple dephosphorylation events), which will allow the dephosphorylation rate in our model to be reduced. In contrast, activation events that require protein recruitment cannot be so grouped. We also used the total number of fully activated TCRs as a measure of system (cell) activation, the accumulation of fully activated TCRs functioning as a signal integrator. Other outputs could easily be used, for instance, sustained internal calcium levels retain transcription factors such as NFAT and NFκB in the nucleus and thereby integrate TCR triggerings. We note that the stability of the sequestered state was essential for signal integration since the inactivation rate α_- directly determined the equilibrium level of fully activated TCRs, and a less stable complex would result in an increased level of noise in the output. Thus, our output has two sources of noise, first the signal noise, i.e., from the source of TCR triggerings, and

second from the accumulation of fully activated TCRs. The latter is in fact very noisy, since the equilibrium load is small, 10–25 (Fig. 4), with a relative error of 20–30%, and thus the signaling characteristics can in fact be superior to that indicated here. Other components of the signaling cascade, e.g., the calcium signal, may therefore have higher specificity under appropriate signal integration, for instance, the sequestering of NFκB in the nucleus.

Finally, we note that mathematical models of the immunological synapse (9) indicate that segregation domains have a minimum possible size. This means that very small KRDs are unstable, and thus can only be transient. During the development of the synapse early signals are essential, since in the absence of agonist, receptor segregation does not occur and the immunological synapse does not form (except on dendritic cells), suggesting that patternation is not thermodynamically favored in the absence of agonist. We suggest that thermal fluctuations generate regions of close contact in the contact interface over a range of sizes from nanometers to hundreds of nanometers, such regions having gross kinase activity, and thus lead to TCR activation in the presence of ligand. For the parameters used here, arbitrarily small domains contributed to triggering, size-enhanced signaling occurring only on domains >100 nm in size. These signals alter the thermodynamic properties of the interface, e.g., upregulation of the adhesion receptor LFA1 affinity, which induces stable receptor segregation as predicted by the mathematical models (9,10). Provided KRDs of sufficient size are seeded during this early stage, patternation will be observed. Thus the size stability threshold is not inconsistent with initial triggering being predominantly through small KRDs.

Z.L. is partially supported by Biotechnology and Biological Sciences Research Council/Engineering and Physical Sciences Research Council grant GR/S29256/01 and Biotechnology and Biological Sciences Research Council grant 88/E17188. P.A.v.d.M. is supported by the Medical Research Council.

REFERENCES

1. Krogsgaard, M., Q. J. Li, C. Sumen, J. B. Huppa, M. Huse, and M. M. Davis. 2005. Agonist/endogenous peptide-MHC heterodimers drive T cell activation and sensitivity. *Nature*. 434:238–243.
2. Gil, D., W. W. A. Schamel, M. Montoya, F. Sanchez-Madrid, and B. Alarcon. 2002. Recruitment of Nck by CD3 epsilon reveals a ligand-induced conformational change essential for T cell receptor signaling and synapse formation. *Cell*. 109:901–912.
3. Gil, D., A. G. Schrum, B. Alarcon, and E. Palmer. 2005. T cell receptor engagement by peptide - MHC ligands induces a conformational change in the CD3 complex of thymocytes. *J. Exp. Med.* 201: 517–522.
4. Davis, S. J., and P. A. van der Merwe. 1996. The structure and ligand interactions of CD2: implications for T-cell function. *Immunol. Today*. 17:177–187.
5. Werlen, G., and E. Palmer. 2002. The TCR signalosome: a dynamic structure with expanding complexity. *Curr. Opin. Immunol.* 14:299–305.
6. Hopfield, J. J. 1974. Kinetic proofreading: a new mechanism for reducing errors in biosynthetic processes requiring high specificity. *Proc. Natl. Acad. Sci. USA*. 71:4135–4139.
7. McKeithan, T. W. 1995. Kinetic proofreading in T-cell receptor signal transduction. *Proc. Natl. Acad. Sci. USA*. 92:5042–5046.
8. Rabinowitz, J. D., C. Beeson, D. S. Lyons, M. M. Davis, and H. M. McConnell. 1996. Kinetic discrimination in T-cell activation. *Proc. Natl. Acad. Sci. USA*. 93:1401–1405.
9. Burroughs, N. J., and C. Wülfing. 2002. Differential segregation in a cell:cell contact interface: the formation of the immunological synapse. *Biophys. J.* 83:1784–1796.
10. Qi, S. Y., J. T. Groves, and A. K. Chakraborty. 2001. Synaptic pattern formation during cellular recognition. *Proc. Natl. Acad. Sci. USA*. 98: 6548–6554.
11. Lee, K. H., A. D. Holdorf, M. L. Dustin, A. C. Chan, P. M. Allen, and A. S. Shaw. 2002. T cell receptor signaling precedes immunological synapse formation. *Science*. 295:1539–1542.
12. Chan, C., A. J. T. George, and J. Stark. 2001. Cooperative enhancement of specificity in a lattice of T cell receptors. *Proc. Natl. Acad. Sci. USA*. 98:5758–5763.
13. Chan, C., J. Stark, and A. J. T. George. 2004. Feedback control of T-cell receptor activation. *Proc. R. Soc. Lond. B. Biol. Sci.* 271:931–939.
14. Dembo, M., D. C. Torney, K. Saxman, and D. Hammer. 1988. The reaction-limited kinetics of membrane-to-surface adhesion and detachment. *Proc. R. Soc. Lond. B. Biol. Sci.* 234:55–83.
15. Wedagedera, J. R., and N. J. Burroughs. 2006. T cell activation: a queueing theory analysis at low agonist density. *Biophys J*. In press.
16. Faroudi, M., R. Zaru, P. Paulet, S. Müller, and S. Valitutti. 2003. Cutting edge: T lymphocyte activation by repeated immunological synapse formation and intermittent signaling. *J. Immunol.* 171:1128–1132.
17. Huppa, J. B., M. Gleimer, C. Sumen, and M. M. Davis. 2003. Continuous T cell receptor signaling required for synapse maintenance and full effector function. *Nat. Immunol.* 4:749–755.
18. Valitutti, S., S. Muller, M. Cella, E. Padovan, and A. Lanzavecchi. 1995. Serial triggering of many T-cell receptors by a few peptide-MHC complexes. *Nature*. 375:148–151.
19. Stotz, S. H., L. Bolliger, F. R. Carbone, and E. Palmer. 1999. T cell receptor (TCR) antagonism without a negative signal: evidence from T cell hybridomas expressing two independent TCRs. *J. Exp. Med.* 189:253–263.
20. Coombs, D., A. M. Kalergis, S. G. Nathenson, C. Wofsy, and B. Goldstein. 2002. Activated TCRs remain marked for internalisation after dissociation from pMHC. *Nat. Immunol.* 3:926–931.
21. Kersh, G. J., E. N. Kersh, D. H. Fremont, and P. M. Allen. 1998. High- and low-potency ligands with similar affinities for the TCR: the importance of kinetics in TCR signaling. *Immunity*. 9:817–826.
22. Lyons, D. S., S. A. Lieberman, J. Hampl, J. Boniface, Y. Chien, L. J. Berg, and M. M. Davis. 1996. A TCR binds to antagonist ligands with lower affinities and faster dissociation rates than to agonists. *Immunity*. 5:53–61.
23. Stefanova, I., B. Hemmer, M. Vergelli, R. Martin, W. E. Biddison, and R. N. Germain. 2003. TCR ligand discrimination is enforced by competing ERK positive and SHP-1 negative feedback pathways. *Nat. Immunol.* 4:248–254.
24. Chan, C., A. J. T. George, and J. Stark. 2003. T cell sensitivity and specificity - kinetic proof reading revisited. *Discrete Contin. Dynam. Syst.*, 3:343–360,.
25. Li, Q.-J., A. R. Dinner, S. Qi, D. J. Irvine, J. B. Huppa, M. M. Davis, and A. K. Chakraborty. 2004. CD4 enhances T cell sensitivity to antigen by coordinating Lck accumulation at the immunological synapse. *Nat. Immunol.* 8:791–799.
26. Williams, A. F., and A. N. Barclay. 1986.Glycoprotein antigens of the lymphocyte surface and their purification by antibody affinity chromatography. *In* Handbook of Experimental Immunology. D. M. Weir, L. A. Herzenberg, C. Blackwell, and L. A. Herzenberg, editors. Blackwell Scientific, 22.1–22.4.
27. Mustelin, T., K. M. Coggeshall, and A. Altman. 1989. Rapid activation of the T-cell tyrosine protein kinase pp56lck by the CD45

phosphotyrosine phosphatase. *Proc. Natl. Acad. Sci. USA*. 86:6302–6306.

28. Tonks, N. K., and B. G. Neel. 2001. Combinatorial control of the specificity of protein tyrosine phosphatases. *Curr. Opin. Cell Biol.* 13: 182–195.
29. Hermiston, M. L., Z. Xu, and A. Weiss. 2003. CD45: a critical regulator of signaling thresholds in immune cells. *Annu. Rev. Immunol.* 21:107–137.
30. Irles, C., A. Symons, F. Michel, T. R. Bakker, P. A. van der Merwe, and O. Acuto. 2003. CD45 ectodomain controls interaction with GEMs and Lck activity for optimal TCR signaling. *Nat. Immunol.* 296:189–197.
31. Lin, J., and A. Weiss. 2003. The tyrosine phosphatase CD148 is excluded from the immunologic synapse and down-regulates prolonged T cell signaling. *J. Cell Biol.* 162:673–682.
32. Wülfing, C., C. Sumen, M. D. Sjaastad, L. C. Wu, M. L. Dustin, and M. M. Davis. 2002. Costimulation and endogenous MHC ligands contribute to T cell recognition. *Nat. Immunol.* 3:42–47.
33. Choudhuri, K., D. Wiseman, M. H. Brown, K. Gould, and P. A. van der Merwe. 2005. T-cell receptor triggering is critically dependent on the dimensions of its peptide-mhc ligand. *Nature*. 436:578–582.
34. Anderson, R. G. W., and K. Jacobson. 2002. A role for lipid shells in targeting proteins to caveolae, rafts, and other lipid domains. *Science*. 296:1821–1825.
35. Kersh, E. N., A. S. Shaw, and P. M. Allen. 1998. Fidelity of T cell activation through multistep T cell receptor zeta phosphorylation. *Science*. 281:572–575.
36. Favier, B., N. J. Burroughs, L. Wedderburn, and S. Valitutti. 2001. T cell antigen receptor dynamics on the surface of living cells. *Int. Immunol.* 13:1525–1532.